This is the Pre-Published Version.

S. Wang#, S. Lin#, Y. Liu, X. Huang*, M.J. Gollner (2022) *Smoldering Ignition using a Concentrated Solar Irradiation Spot*, **Fire Safety Journal**, 128, 103549. https://doi.org/10.1016/j.firesaf.2022.103549

Smoldering Ignition using a Concentrated Solar Irradiation Spot

Siyan Wang[1,#], Shaorun Lin[1,2,#], Yanhui Liu[1,2], Xinyan Huang[1,2,*], Michael J. Gollner[3]

[1]*Research Centre for Fire Safety Engineering, The Hong Kong Polytechnic University, Hong Kong*

[2]*The Hong Kong Polytechnic University Shenzhen Research Institute, Shenzhen, Guangdong, China*

[3]*Deparment of Mechanical Engineering, University of California, Berkeley, CA, USA*

[#] *Joint first author, these authors contributed equally to this study.*

**Corresponding author: xy.huang@polyu.edu.hk*

Abstract:

Ignition of materials by a point source of heating plays an important role in initiating many structure and wildland fires, such as spotting by hot particles, lightning, laser, and concentrated irradiation. Herein, we study the smoldering ignition of tissue paper by a concentrated sunlight spot with heat fluxes up to 780 kW/m^2, which is focused by a transparent glass sphere. The diameter of the sunlight spot on the paper sample ranges from 1.5 to 20.0 mm by varying the paper position within the focal length, where a smaller spot has a larger intensity of sunlight irradiation. The measured minimum spot irradiation for smoldering ignition is not a constant but is much higher than 11 kW/m^2 measured in a traditional cone-calorimeter test. As the diameter of the irradiation spot decreases from 20 to 1.5 mm, the minimum irradiation for smoldering ignition increases from 17.5 to 205 kW/m^2, and the ignition energy increases from 0.084 to 2.0 MJ/m^2. A simplified heat transfer analysis reveals that the lateral conductive cooling within the fuel becomes dominant for a smaller spot ignition area. This work ultimately quantifies the potential fire risk from concentrated sunlight spots and helps elucidate the underlying mechanisms leading to smoldering ignition.

Keywords: Smoldering combustion; Point heating; Critical irradiation; Ignition energy; Sunlight spot.

1. Introduction

The ignition of combustible materials is fundamental to fire safety analyses, defining initiation and leading to the eventual growth of sometimes devastating fire events. Many ignition events leading to both structure and wildland fires occur remotely by a point heating source [1], such as the deposition of lofted firebrands [2–4], hot metal particles [4,5], dripping molten materials [6], laser irradiation [7–10], lightning strikes [11], and concentrated irradiation [12–15]. Significant studies have recently focused on spotting ignition of various fuels by lofted firebrands, which can sometimes dominate the fire spread rate in both wildland and wildland-urban interface (WUI) fires [2,3]. A lesser-studied source of ignition is a concentrated sunlight spot, which can be reflected by a curved mirror or focused by a dew droplet, curved glass window and decorations, transparent fish bowls, or cylindrical bottles filled with water [16–18]. From 2010 to 2015, 125 fires in the United Kingdom were reported to be triggered by a concentrated sunlight spot [19], posing threats to both human lives and property. However, to the best of the authors' knowledge, this remote ignition phenomenon has not received a detailed and quantitative study, presenting a key knowledge gap.

Nomenclature

Symbols		***Greeks***	
Bi	Biot number (-)	α	thermal diffusivity (m^2/s)
c_p	specific heat (J/kg-K)	ε	emissivity (-)
C	concentration factor (-)	σ	Stefan-Boltzmann constant (J/m^2-s-K^4)
D	light spot diameter (m)	δ	thickness (m)
D_{O_2}	oxygen diffusivity (m^2/s)	ρ	density (kg/m^3)
E_{ig}	ignition energy (MJ)		
E''_{ig}	ignition energy per unit area (MJ/m^2)	***Subscripts***	
h	heat transfer coefficient ($W/(m^2K)$)	∞	ambient
k	thermal conductivity ($W/(mK)$)	*c*	concentrated
n_c	refractive index (-)	*cond*	conduction
$\dot{q}''$	heat flux (kW/m^2)	*crt*	critical
r	radius (m)	*ig*	ignition
Δr	thermal penetration depth (m)	*min*	minimum
T	temperature (°C/K)	*s*	solar
ΔT	temperature difference (°C/K)	*sm*	smoldering
t	time (s)	*T*	thermal

Over the past 50 years, limited studies have investigated flaming ignition by a laser spot or concentrated irradiation. Kashiwagi [7,8] showed that the minimum radiant heat fluxes for flaming autoignition are 90 kW/m^2 for red oak and 160 kW/m^2 for PMMA, performed with a 2-3 cm diameter laser spot. By increasing the diameter of the heating spot to about 3.5 cm, the minimum radiant fluxes decreased to 80-90 kW/m^2, still much higher than a value of 25-50 kW/m^2 reported for auto-ignition of 10-cm width square wood samples more evenly heated in a cone calorimeter [20]. Later, the laser ignition of thin PMMA sheets with different orientations has also been investigated experimentally and numerically [21,22]. Grishin et al. [12] generated a light beam by a tungsten lamp to ignite a porous forest fuel layer with a bulk density of 6-24 kg/m^3 and revealed that the required irradiant heat flux for flaming ignition decreases as the heating diameter increases from 8 mm to 27 mm. Warren [13] concentrated sunlight using a spherical water-filled glass bowl with a diameter of 200 mm and demonstrated the possibility of smoldering ignition of print paper by concentrated irradiation. Recently, Sandia National Laboratories [14,15] used hundreds of reflection mirrors in a concentrated solar tower plant to generate an irradiation greater than 2,000 kW/m^2 (about 0.5-m diameter spot) that could ignite some common fuels within a few seconds.

Compared to spotting ignition by direct contact with a hot metal spark or firebrand (i.e., transfer of both a physical heat source and fuel) [2,4], ignition by a concentrated irradiation spot involves only energy transfer. Thus, such an ignition process is simpler, which may also provide valuable information applicable to other

spotting ignition processes. Once an intense irradiation spot is applied, a recipient fuel may first be heated, dried, decompose, and then begin to smolder. Auto-ignition directly to a flaming mode of combustion is also possible if the radiation is strong enough [8,23]. Smoldering combustion is slow, low-temperature and flameless burning of porous fuel, which is sustained as a heterogeneous oxidative process and different from flaming combustion [24]. Smoldering is a common fire phenomenon in both structures and wildland, such as the burning of upholstered furniture, mattresses, firebrands, duff, and peatlands [24–26]. Smoldering can be easily initiated by a weaker ignition source or even self-ignited, providing a shortcut to severe fire events through the smoldering-to-flaming transition [24,25,27–30]. Therefore, it is of vital significance to fully understand smoldering ignition. So far, little research has studied the smoldering ignition by concentrated irradation spots, and the ignition criteria are still poorly understood.

This work investigates the smoldering ignition of multiple-layered tissue paper samples by intense point irradiation, i.e., a sunlight spot concentrated by a spherical glass ball. Within the focus length, the diameter of the heating spot was varied from 1.5 mm to 20 mm, and the intensity of irradiation was varied up to 780 kW/m^2. The ignition delay time, critical heat flux, and ignition energy of smoldering by the irradiation spot were quantified. Finally, a simplified heat transfer model was proposed to (1) explain the varying minimum irradiation and energy required for smoldering ignition and (2) quantify the potential ignition risk initiated by the concentrated sunlight in both structure and wildland fires.

2. Experimental methods

2.1. Materials and apparatus

Thin tissue paper made of unbleached pulp was used in the experiment, as it was a typical thin fuel that could be found in residential buildings and similar in nature to cellulosic wildland fuels. The results of thermogravimetric analysis (TGA) could be found in Appendix (Fig. A1). Before the test, the tissue paper was first oven-dried at 75 ℃ for 48 h, and its dried bulk density was measured to be 98 ± 5 kg/m^3. Afterward, it was placed into an electronic dry cabinet to avoid re-absorption of moisture from the air. For the test, the tissue was first cut into a size of 60 mm × 60 mm, and six layers of tissue were packed into a sample with an overall thickness (δ) of about 2 mm (see Fig. 1a). For a single layer of tissue (about 0.1-mm thick), the concentrated irradiation spot would create a hole on the tissue directly without ignition, so multiple layers of tissue were used. The gap between layers was minimized to consider the total sample as one, and the influence of the gap between layers was characterized by the bluk density.

In the experiment, natural sunlight was concentrated by a 150-mm K9 crown glass sphere with a refractive index (n_c) around 1.53. The spherical lens minimized the operation of the concentrator during the experiment, because its projection of sunlight beam was fixed and insensitive to the position of the sun. The focal length and back focal length of the crown glass sphere were theoretically calculated to be 108 mm and 33 mm [31], as illustrated in Fig. 1b.

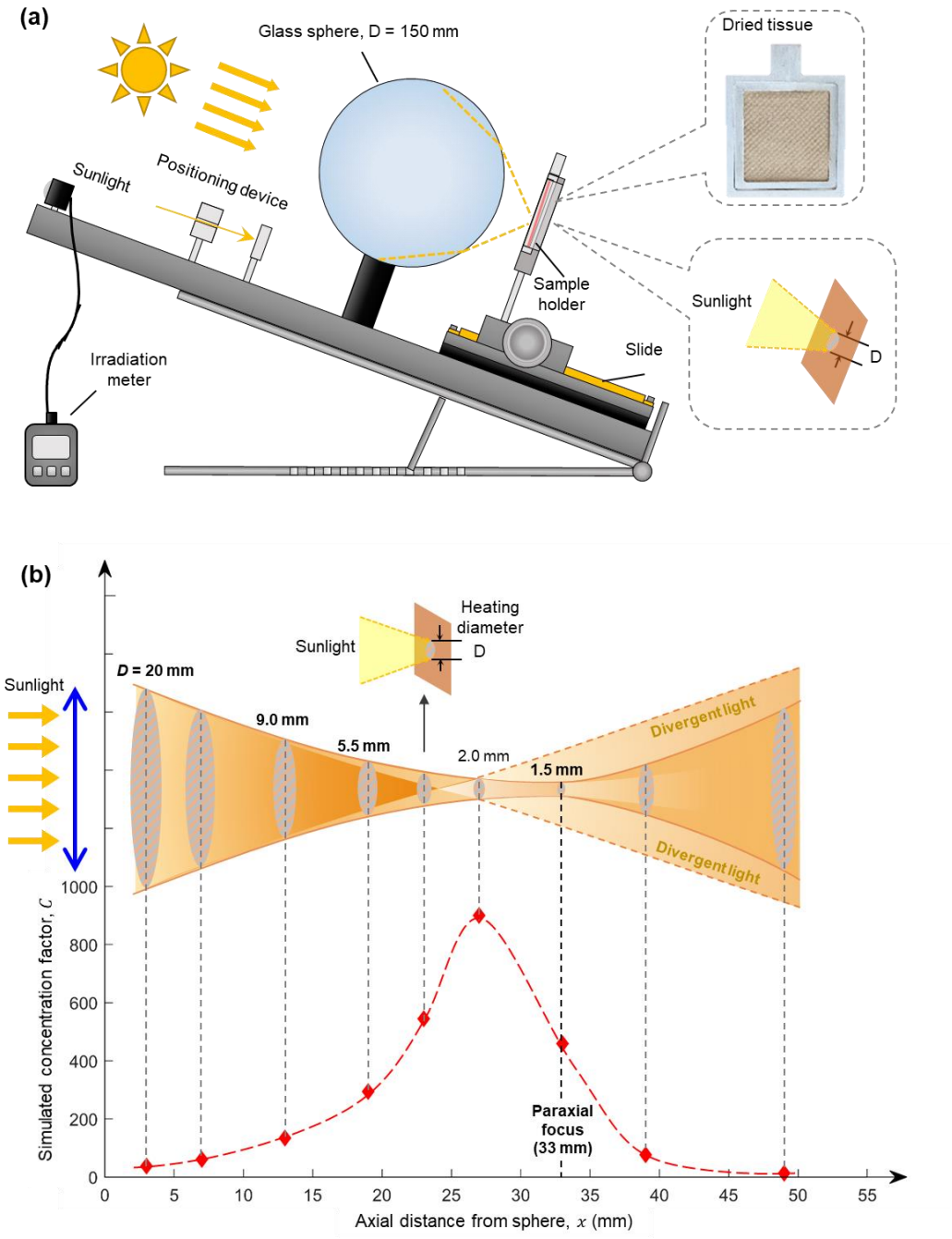

Fig. 1. (a) Schematic diagram of the designed experiment apparatus, and (b) overall concentration factor at different axial distance from sphere.

A positioning device was fixed perpendicular to the surface of the base stand (Fig. 1a). To ensure that the device was parallel to the sunlight, the angle of the base stand was adjusted until the light beam passed through the hole in the middle of the front aluminum block and projected on the middle of the back aluminum block. A solar power meter was fixed at the front towards the sunlight direction to record real-time solar irradiation ($\dot{q}_s''$). The sample frame was a hollow box that provided a volume of 60 × 60 × 2 mm^3 for the tissue sample and was inserted into the sample holder. The sample holder was installed on a slide that can adjust its distance between the tissue sample and the glass sphere with a precision of 0.5 mm.

2.2. Irradiant heat flux of concentrated light spot

Traditionally, the value of incident irradiant heat flux can be measured by a radiometer. However, as the diameter of the light spot decreases, the heat flux of sunlight concentrated by the glass sphere could exceed 500 kW/m^2, which was much higher than the upper limit (usually 100-200 kW/m^2) of a conventional radiometer. Thus, to quantify the high irradiation of concentrated sunlight spot, an optical simulation performed in *TracePro* [32] was first used to correlate the size of the light spot and theoretical irradiation ($\dot{q}_c''$) concentrated by a 150-mm crown glass sphere.

In the optical simulation, the overall concentration factor (C) is a ratio of irradiation level after and before concentrating which could be used to quantify the concentrated irradiation flux in this study. The overall concentration factor considered not only optical concentration, but also the actual energy dissipation, such as the light reflected, refracted, and absorbed by the glass sphere in the transmitting process [13].

Fig. 1b shows the overall concentration factor (C) vs. light spot diameter (D) of a 150-mm glass sphere based on an optical simulation performed in *TracePro* [32]. Note that the peak concentration factor is about 900 at about D = 2 mm, which is not at the optical back focal length. Due to losses resulting from reflection, refraction, and spherical aberration, the concentration factor of the smallest light spot (D = 1.5 mm) is about 460 at the back focal length.

With the instant solar irradiation ($\dot{q}_s''$) and the overall concentration factor (C) for different light spots determined, the actual concentrated solar irradiant heat flux to the fuel sample can be calculated as

$$\dot{q}_c'' = C\dot{q}_s'' \tag{1}$$

For example, if the solar irradiation is 1 kW/m^2 [33], the resultant heat flux peaks at around 900 kW/m^2, which is close to the literature value [13]. In addition, the conventional radiometer was used to measure the concentrated solar irradiation of large spots up to 200 kW/m^2 and compare with the calculated values by Eq. (1) in Fig. A2. Good agreement was found between the radiometer and calculated values, confirming the accuracy of the irradiation heat flux based on the optical simulation.

Table 1. Summary of diameters of the concentrated irradiation spots (D) and concentration factors (C) at different distances from the glass sphere.

Distance from sphere, x (mm)	**33.0**	**19.0**	**13.0**	**3.0**
Irradiation spot diameter, D (mm)	1.5	5.5	9.0	20
Concentration factor, C	460	294	134	38

Sunlight through the glass sphere will also form a caustic zone instead of a focal point due to the existence of spherical aberration, that is, the blurry appearance of the outer part of the view of a convex lens [15]. As the spots become intensively blurry beyond the focus length, their edge could be hard to identify. Therefore, to maintain better precision, only light spots within the back focal length with clearly defined boundary were adopted in the experiment [34]. In total, four different positions (x) of 3 mm, 13 mm, 19 mm, and 33 mm within

the glass sphere's back focal length were tested, with respect to four heating diameters (D) of 20.0 mm, 9.0 mm, 5.5 mm, and 1.5 mm, as summarized in Table 1.

2.3. Experimental procedures

Before the test, the diameter of the light spot was adjusted by controlling the distance between the glass sphere and sample. Afterward, the light spot was shielded by a piece of black cardboard, and the tissue sample was inserted into the sample holder. Once the solar irradiation heat flux ($\dot{q}_s''$) read by the solar power meter was relatively constant, the back cardboard was removed to allow the light spot to irradiate the fuel surface. Then, the sample was heated by the light spot for a prescribed duration (t).

For flaming ignition, the time of ignition can be determined by the appearance of a flame. However, it was not possible to instantaneously determine the success of smoldering ignition and the exact ignition time [28]. Thus, the tissue sample was first heated for a prescribed duration, and then it was left in the controlled environment without wind for another 5 min for further observation. Successful smoldering ignition was then identified if the smoldering spot was self-sustaining. A self-sustained smoldering is defined as the smoldering front successfully propagating outwards from the heating region within 5 min, eventually burning out the sample. If smoldering ignition was not observed, the heating duration was increased until smoldering ignition was successful. Then, more than 100 tests were conducted using the same heating diameter under a range of concentrated irradiations. Afterward, the diameter of the heating spot was varied by moving the sample within the focal length to investigate its effect on smoldering ignition.

In total, more than 600 tests were conducted outdoors on typical summer sunny days with a clear blue sky. Depending on the weather and solar zenith angle, the instant solar radiation ranged from 0.2 kW/m^2 (at nightfall) to 1.6 kWm^2 (at noon). During the test, the ambient temperature was 29 ± 2 °C, the relative humidity was 82 ± 10 %, the wind speed was 5.5 ± 0.9 m/s, and the ambient pressure was 101 kPa.

3. Results and discussion

3.1. Smoldering spotting ignition phenomena

Fig. 2a shows an example of a successful smoldering ignition process by a concentrated irradiation spot with a diameter of 1.5 mm and a resultant irradiation heat flux of 560 kW/m^2. Once the irradiation spot was applied on the sample surface, some smoke was released, likely a combination of condensed water vapor and pyrolysis gases [28]. Continuing the heating, the surface layer within the light spot turned black (or charred) and cracked, allowing the light beam to heat the lower layers directly. After heating for about 8 s, the sample detached from the apparatus but remained in the controlled environment (without wind) for another 5 min. As a result, the black spot expanded outwards evenly, expanding at a stable rate, and eventually burned out the sample. Fig. 2b shows an example of a failed smoldering ignition process by the concentrated irradiation spot with a diameter of 1.5 mm and a resultant radiant heat flux of 300 kW/m^2. Initially, smoke and a charring tendency were also observed. However, after heating for 8 s, no smoldering propagation phenomenon was observed, indicating a failed ignition. More videos can be found in the *Supplementary Materials* (Videos S1-2).

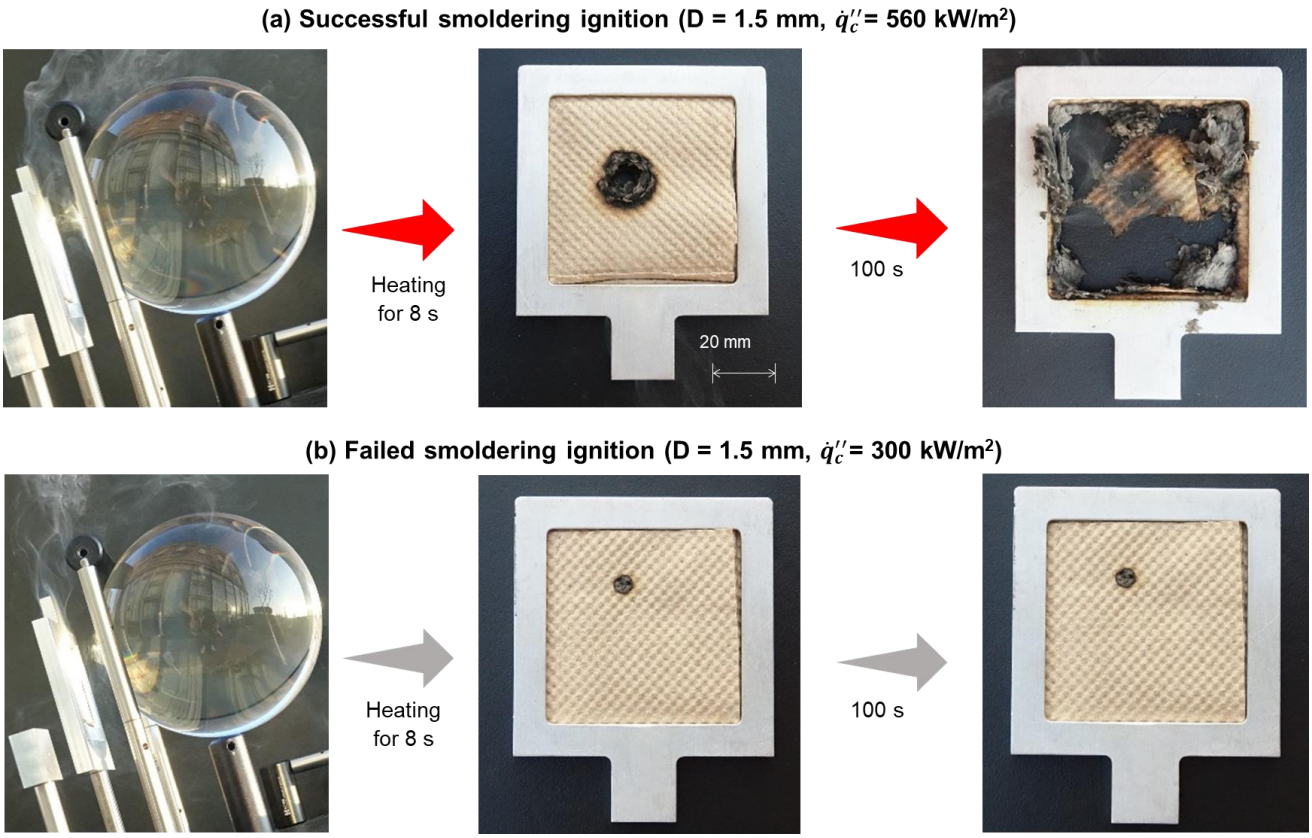

Fig. 2. Smoldering ignition of dried tissue samples by concentrated irradiation spot with a diameter of 1.5 mm for 8 s, (a) successful ignition under irradiation of 560 kW/m^2, and (b) failed ignition under irradiation of 300 kW/m^2.

3.2. Irradiation duration for ignition and critical irradiation

The experimental outcomes under different diameters of concentrated irradiation spots (D) and the resultant irradiant heat fluxes ($\dot{q}_c''$) are summarized in Fig. 3, where the solid and hollow markers represent failed and successful ignition, respectively. Note that the instant solar radiation ($\dot{q}_s''$) changed from time to time, so there was a large scattering in the irradiation value. Given the diameter of the concentrated irradiation spot, the required heating duration for the smoldering ignition (t_{ig}) decreases as the external irradiation increases. This trend is similar to the piloted flaming ignition theory, where the flaming ignition time is mainly the required heating time for pyrolysis [25,28].

In general, the required duration for smoldering ignition (t_{ig}) is the time to heat the fuel surface to a critical smoldering temperature (T_{sm}) which is the threshold temperature of char oxidation [28]. For a typical 1-D thermally-thin material (i.e., small Biot number $Bi < 0.1$), if heat transfer inside the fuel is neglected, the ignition time can be approximated as

$$t_{ig} \approx \frac{\rho c_p \delta (T_{sm} - T_0)}{\dot{q}_c'' - \dot{q}_{crt}''} \tag{2}$$

where ρ, c_p, and δ are the density, specific heat, and thickness of fuel, respectively; T_0 is the initial fuel temperature; and $\dot{q}_{crt}''$ is the critical heat flux for smoldering ignition.

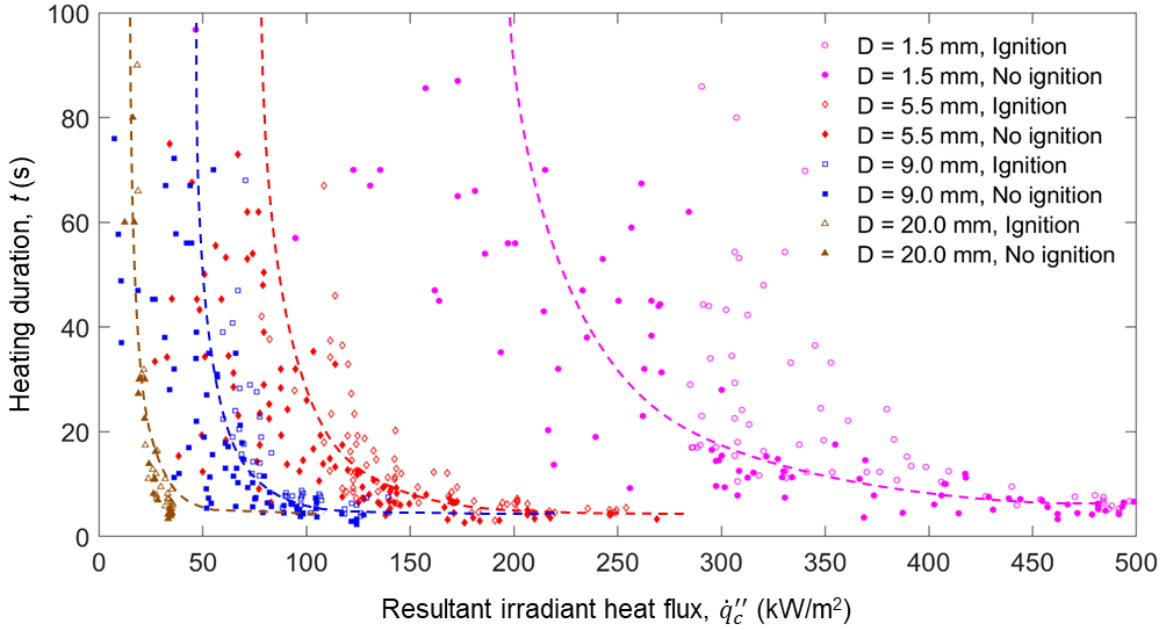

Fig. 3. The experimental outcomes under different diameters of irradiation spots (D) and the resultant irradiant heat fluxes ($\dot{q}_c''$), where the solid and hollow markers represent failed and successful ignition, respectively.

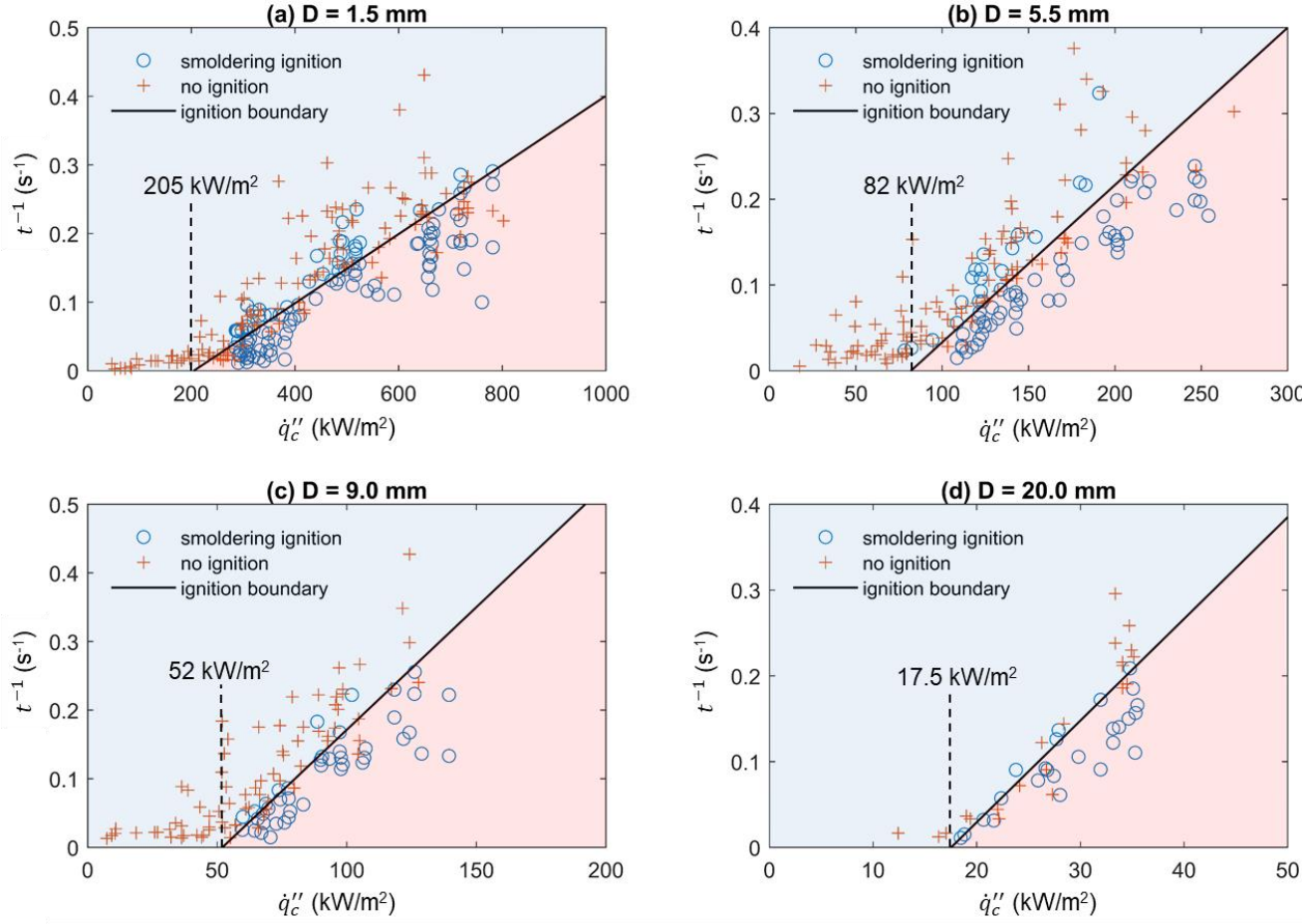

Fig. 4. The relationship between t^{-1} and $\dot{q}_c''$ under different spot diameters and the critical irradiation levels, where the fitting curves of ignition boundaries were obtained from the logistic regression model.

Fig. 4 further verifies the relationships between t^{-1} and $\dot{q}_c''$ with different diameters of the concentrated irradiation spots, where the linear correlations of the ignition boundaries (i.e., t_{ig}) were obtained from the logistic regression model [35]. The performances of this statistical model were speculated and could be found in the Appendix. Based on Eq. (2), the critical heat flux for smoldering ignition ($\dot{q}_{crt}''$) can be estimated by a linear extrapolation of ignition boundary towards the x-axis (i.e., $t_{ig} \to \infty$), as indicated in Fig. 4. Interestingly, as the diameter of concentrated irradiation spot decreases from 20 mm to 1.5 mm, the critical heat flux increases dramatically from 18 kW/m^2 to 205 kW/m^2 (see the summary in Table 2).

Fig. 5a further plots the critical irradiation heat fluxes for smoldering ignition vs. the spot diameters. For a larger irradiation spot, the critical irradiation of ignition is low. Due to losses resulting from reflection, refraction, and spherical aberration, it is extremely difficult to find the exact position of low irradiation level within the focus length, which could also result in a large uncertainty. Therefore, the cone calorimeter was applied here to provide a reference value with a larger heating spot (i.e., D=60 mm). Clearly, as the diameter of the irradiation spot increases, the critical heat flux for smoldering ignition decreases, and eventually, it approaches a near-minimum value obtained from the cone calorimeter (about 11 kW/m^2).

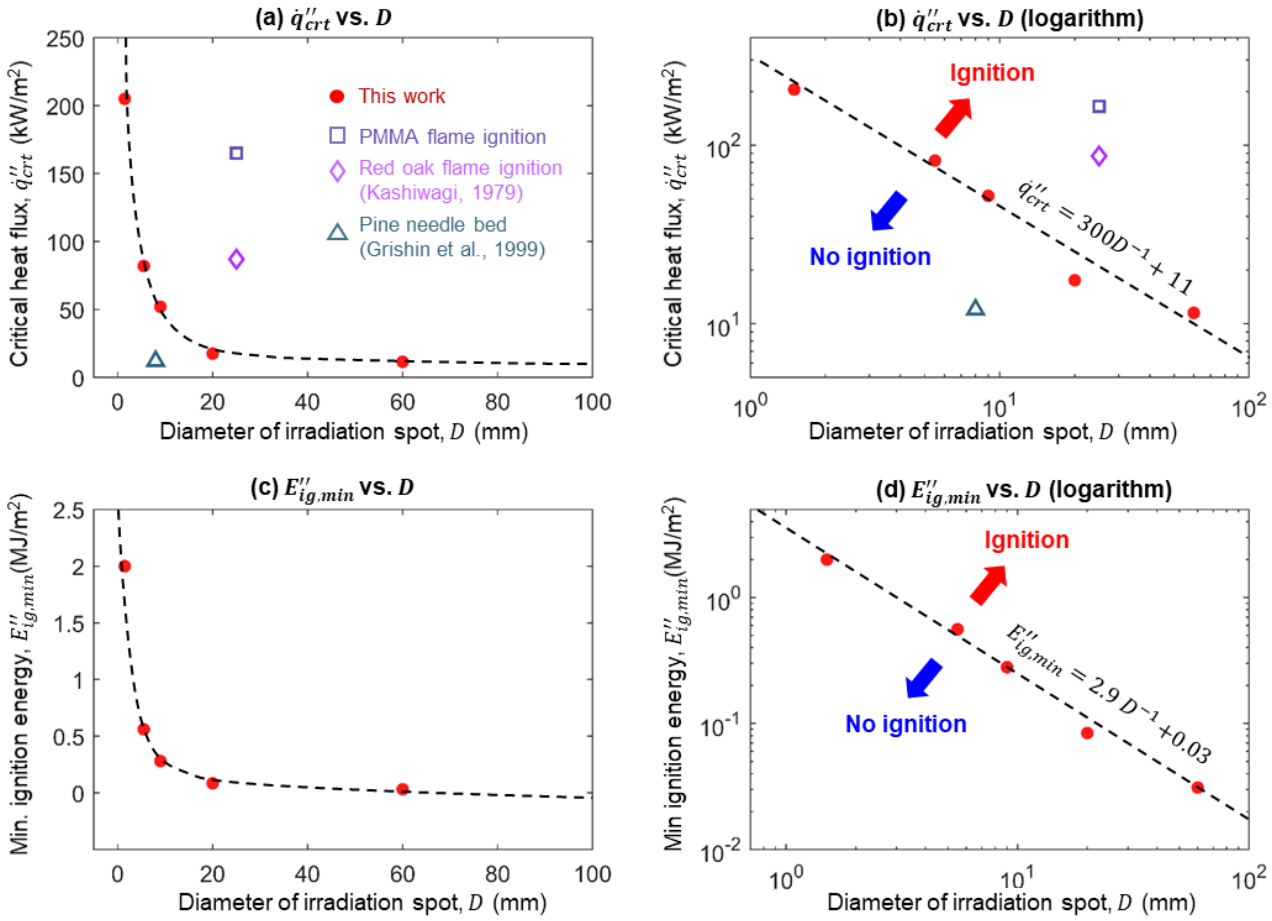

Fig. 5. The relationship between diameters of irradiation spots (D) and (a-b) critical ignition heat fluxes ($\dot{q}_{crt}''$); and (c-d) smoldering ignition energy ($E_{ig,min}''$), where the laser ignition data of PMMA and red oak sheet are from Kashiwagi [7], and data of the pine needle bed are from Grishin et al. [12].

As a reference, critical heat fluxes for flaming auto-ignition of the 12-mm thick PMMA sheet and the 17-mm thick red oak wood by a 25-mm laser spot [7] and a loose pine needle bed (~20 kg/m^3) by a light beam [12] are also plotted in Fig. 5a. In general, the critical irradiation heat flux only slightly varies with the thickness of the fuel sample when irradiant heating and environmental cooling (including some radiation obsorption by pyrolysis gases [7]) reach a balance, thus ensuring an acceptable comparison. As expected, under the same irradiation-spot size (25 mm), a much large irradiation heat flux is needed to achieve a flame auto-ignition [7]. For very porous pine needles, the smoldering ignition was first achieved and then transitioned to a flame [12]. More importantly, the absorption of irradiation by a porous fuel was a volumetric process, which is more effective than the surface absorption by a more compact tissue in this work, so its critical irradiation heat flux for smoldering ignition was smaller.

For the current experiments, an empirical correlation between the critical heat flux ($\dot{q}''_{crt}$) for smoldering ignition and the diameter of concentrated irradiation spot (D) can be formulated as

$$\dot{q}''_{crt} = 11 + \frac{300}{D} \tag{3}$$

where units of [kW/m^2] for $\dot{q}''_{crt}$ and [mm] for D are used. Excellent linearity is found using logarithmic coordinates in Fig. 5b, with an R^2 coefficient of 0.97, indicating a strong power-law correlation.

Table 2. Summary of critical heat flux ($\dot{q}''_{crt}$) and minimum ignition energy ($E''_{ig,min}$) for smoldering spotting ignition with different light spot diameters.

Irradiation spot diameter, *D* (mm)	**1.5**	**5.5**	**9.0**	**20**	**60***
Critical irradiation for ignition, $\dot{q}''_{c,crt}$ (kW/m^2)	205	82	52	17.5	11.5
Minimum ignition energy, $E''_{ig,min}$ (MJ/m^2)	2.0	0.56	0.28	0.084	0.031

*The whole 60 mm × 60 mm sample was tested under the irradiation of the cone calorimeter.

3.3. Ignition energy

The smoldering ignition energy per unit area (E''_{ig}) for the thin tissue sample provided by the concentrated irradiation can be approximately calculated as

$$E''_{ig} = \dot{q}''_c t_{ig} \approx \rho c_p \delta (T_{sm} - T_0) \frac{\dot{q}''_c}{\dot{q}''_c - \dot{q}''_{crt}} \tag{4}$$

where the minimum heating duration for ignition (t_{ig}) could be obtained from Fig. 4. The smoldering ignition energy for different diameters of the irradiation spot is shown in Fig. 6. As the irradiation level ($\dot{q}''_c$) increases, the ignition time decreases, and the ignition energy gradually decreases, eventually approaching a minimum value [28], as shown in Fig. 6. Then, the minimum ignition energy per unit area of smoldering ($E''_{ig,min}$) can be defined. Eq. (4) suggests that $E''_{ig,min}$ should be a material constant of $\rho c_p \delta (T_{sm} - T_0)$ at $\dot{q}''_c \gg \dot{q}''_{crt}$, which disagrees with the different trendlines in Fig. 6.

Fig. 5c-d further compares the values of $E''_{ig,min}$ for different spot diameters (also see Table 2). As the diameter of the irradiation spot increases from 1.5 mm to 20 mm, the $E''_{ig,min}$ decreases from 2.0 MJ/m^2 to 0.084 MJ/m^2. An empirical correlation between minimum ignition energy flux ($E''_{ig,min}$) and spot diameter (D) can be found as

$$E''_{ig,min} = 0.03 + \frac{2.9}{D} \tag{5}$$

where units of [MJ/m^2] for $E''_{ig,min}$ and [mm] for D are used. An excellent degree of fit (R^2 coefficient of 0.99) can be seen using logarithmic coordinates in Fig. 5d. In other words, both the critical irradiation heat flux and the minimum ignition energy per unit area change with the diameter of irradiation spot, indicating that the conventional 1-D heat transfer analysis becomes invalid for an irradiation spot smaller than 20 mm, even if the fuel is physically thin (but it is no longer thermally thin).

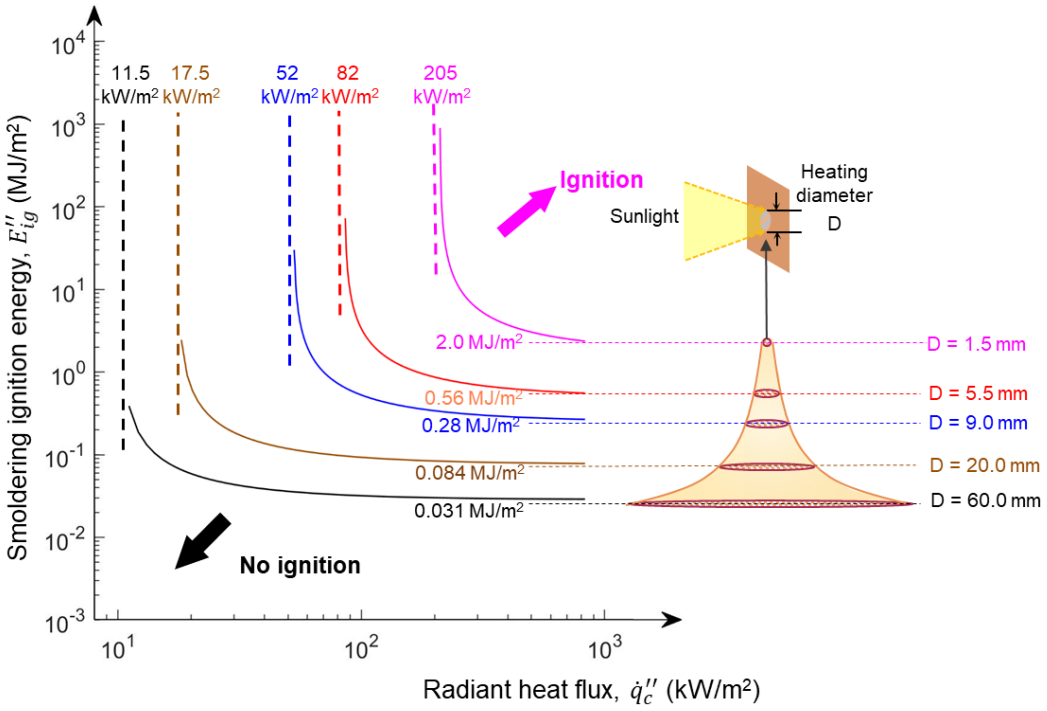

Fig. 6. The relationship between ignition energy (E''_{ig}) and the irradiation heat flux ($\dot{q}''_c$) with different spot diameters (D), where the minimum ignition energy ($E''_{ig,min}$) could be represented as the dashed trendline.

3.4. Theoretical analysis

To scientifically understand the effect of the small irradiation spot on the critical heat flux of smoldering ignition, a characteristic smoldering ignition temperature (T_{sm}) is needed. Such a temperature should be high enough to initiate a robust char oxidation, which ranges from 230 ℃ to 400 ℃, depending on the type and chemistry of fuel [28,36,37]. Then, a simplified 2-D heat transfer analysis based on thermal equilibrium (i.e., the thermally-thin assumption) is proposed for a sample heated by a small irradiation spot, as shown in Fig. 7. Because the diameter of the spot is very small, the conductive cooling outwards from the heating spot perimeter has to be considered.

Therefore, the critical irradiation heat flux for smoldering ignition ($\dot{q}''_{crt}$) should be determined via a balance between the incident radiation, environmental heat losses from the top and back sides ($\dot{q}''_{\infty}$) and the radial conductive heat loss to the virgin fuel ($\dot{q}''_{cond}$) [28,38] at the smoldering temperature (T_{sm}) as

$$\dot{q}''_{crt}\left(\frac{\pi D^2}{4}\right) = \dot{q}''_{\infty}\left(\frac{\pi D^2}{4}\right) \times 2 + \dot{q}''_{cond}(\pi D\delta) \tag{6}$$

which can be further expressed and simplified as

$$\dot{q}''_{crt} = 2\dot{q}''_{\infty} + \frac{4\delta\dot{q}''_{cond}}{D} \qquad \text{(small spot)} \tag{7}$$

Therefore, as the diameter of the irradiation spot increases, the critical heat flux for smoldering ignition decreases, agreeing with the trend in Fig. 5a. Based on the fitting correlation of $\dot{q}''_{crt} = 11 + 300/D$ in Eq. (3), the average conductive heat flux ($\dot{q}''_{cond}$) is found to be 37.5 kW/m^2 approximately, which is much larger than the environmental heat loss ($\dot{q}''_{\infty}$) of 5.5 kW/m^2. Thus, for a small irradiation spot, the internal conductive heat transfer in the solid phase is the dominant heat loss. Note that when the spot diameter is smaller than the paper thickness or the characteristic diffusion length, $\dot{q}''_{cond}$ will also increase due to the curvature effect.

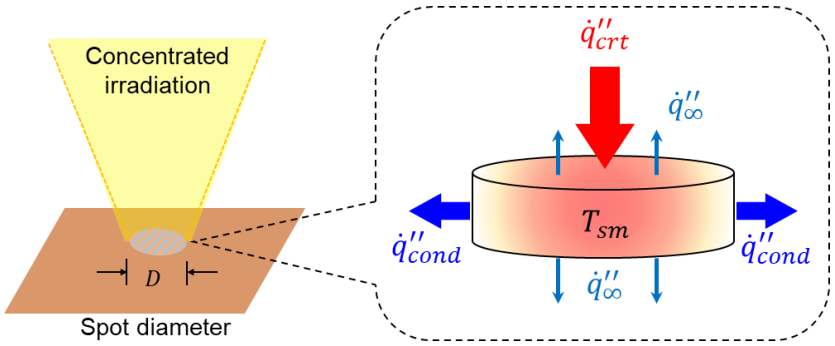

Fig. 7 Schematic diagram of smoldering ignition by concentration irradiation spot, where the critical heat flux for ignition should balance environmental heat loss ($\dot{q}''_{\infty}$) and internal conductive heat loss from the perimeter ($\dot{q}''_{cond}$).

As the diameter of the irradiation spot (D) increases, the effect of conduction in Eq. (7) gradually approaches zero. Thus, for a larger irradiation spot ($D > 17$ mm), heat transfer can be approximated as a conventional 1-D process. The critical heat flux for smoldering ignition then approaches 11 kW/m^2, which approximately equals the environmental heat losses from the top and back surfaces,

$$\dot{q}''_{crt} = 2\dot{q}''_{\infty} = 2[\varepsilon\sigma(T_{sm}^4 - T_{\infty}^4) + h(T_{sm} - T_{\infty})] \quad \text{(large spot)} \tag{8}$$

where $\varepsilon = 0.9$ is the emissivity of the tissue paper, $\sigma = 5.67 \times 10^{-8}$ Jm^{-2}s^{-1}K^{-4} is the Stefan-Boltzmann constant, T_{∞} is the ambient temperature. As a simplification, heat transfer coefficient of $h = 1.52(T_{sm} - T_{\infty})^{1/3}$ for a hot horizontal flat plate is used, considering the large temperature gradient above the hot spot [39]. Therefore, the smoldering ignition temperature can be calculated as $T_{sm} \approx 251$ °C, agreeing with thermal analysis data in the literature [28,36] and Appendix (Fig. A1).

As the irradiation level ($\dot{q}_c''$) increases above 1,000 kW/m^2, the ignition energy flux for smoldering eventually approaches a minimum value ($E_{ig,min}''$ in Fig. 6), which is not a constant but increases as the diameter of irradiation spot decreases (Fig. 5c-d). This primarily occurs because, for a small irradiation spot, the minimum ignition energy needs to not only to heat the fuel up to its ignition temperature (T_{sm}), but also to overcome the large radial conductive heat loss to the surrounding fuel. Thus, the energy balance for the minimum ignition energy can be expressed as

$$E_{ig,min} = \rho c_p \, \delta_T (T_{sm} - T_0) \left(\frac{\pi D^2}{4} \right) + \dot{q}_{cond}'' t_{min} (\pi D \delta_T) \tag{9}$$

where δ_T is the thermal penetrated depth. Then, the required minimum ignition energy per unit area becomes

$$E_{ig,min}'' = \rho c_p \delta (T_{sm} - T_0) + \frac{4 \delta \dot{q}_{cond}'' t_{min}}{D} \tag{10}$$

Therefore, as the diameter of the irradiation spot increases, the minimum ignition energy per unit area for smoldering ignition decreases, agreeing with the fitting correlation of $E_{ig,min}'' = 0.03 + 2.9/D$ in Eq. (5). Based on this experimental fitting correlation and $\dot{q}_{cond}'' \approx 37.5$ kW/m^2 estimated from Eq. (7), the thermal penetration depth could be estimated as $\delta_T = 0.8$ mm and the minimum heating time for smoldering ignition as $t_{min} = 0.024$ s, which is a theoretical limit.

The thermal penetration time (t_T) may also be estimated by heat conduction or thermal diffusion and the oxygen diffusion time (t_{O_2}), which can be estimated as

$$t_T = \frac{\delta^2}{\alpha_p} \approx \frac{\delta^2}{D_{O_2}} \approx 1 \text{ s} \tag{11}$$

where $\alpha_p \approx D_{O_2} \approx 5 \times 10^{-7}$ m^2/s [40] because of the comparable thermal and gas diffusion processes into the paper. The calculated t_T is much larger than the $t_{min} = 0.024$ s estimated from the experimental data. Thus, under an extremely large irradiation heat flux ($\dot{q}_c'' > 1{,}000$ kW/m^2), the limiting time scale may no longer be controlled by the thermal diffusion in the solid fuel, where the diffusion of oxygen is also not fast enough to maintain any smoldering. As observed in the preliminary experiment with a single-layer tissue (0.01 mm), when the irradiation is extremely high, the irradiation spot will break the tissue instantaneously, leaving a hole without any form of ignition. Within such a short period, the super-heated tissue and the formed char are likely to be evaporated within a few milliseconds, so that this process is controlled by gasification chemistry and the thermomechanical resilience of the material, rather than the heat transfer process. Future numerical simulations are needed to reveal more insights on the minimum ignition energy for different fuels and other underlying physical processes.

4. Conclusions

In this work, we investigated the smoldering ignition of multi-layered thin tissue paper by small irradiation spots. Irradiant spots were experimentally generated via concentrating sunlight by a transparent glass sphere

with a diameter of 150 mm and a focal length of 108 mm. To quantify the concentrated radiant heat flux, optical simulations using *TracePro* were conducted to model the diameter of the irradiation spot and the resulting radiation distribution.

We found that as the solar irradiation increases or the diameter of the irradiation spot decreases, the resultant irradiance increases. Given a fixed-size irradiation spot, the smoldering ignition time decreases as the concentrated irradiation increases, following the classical piloted ignition theory. However, the measured minimum spot irradiation for smoldering ignition is not constant but remains much higher than the 11 kW/m^2 measured from cone-calorimeter tests. As the diameter of irradiation spots decreases from 20.0 mm to 1.5 mm, the minimum irradiation necessary for smoldering ignition increases from 17.5 kW/m^2 to 205 kW/m^2, and the ignition energy increases from 0.084 MJ/m^2 to 2.0 MJ/m^2.

A simplified heat transfer analysis was proposed, which explains the critical smoldering ignition heat flux and the minimum ignition energy for tiny irradiation spots by including two-dimensional cooling effects. Future numerical simulations are needed to further reveal the underlying physical and chemical process of smoldering spot ignition for other fuels.

CRediT authorship contribution statement

Siyan Wang: Investigation, Writing-original draft, Formal analysis; **Shaorun Lin**: Investigation, Writing-review & editing, Formal analysis; **Yanhui Liu:** Investigation, Resources; **Xinyan Huang:** Conceptualization, Supervision, Writing-review & editing, Funding acquisition; **Michael J. Gollner:** Writing-review & editing, Supervision.

Conflicts of interest

The authors declare that they do not have any conflicts of interest.

Acknowledgments

This research is funded by the National Natural Science Foundation of China (NSFC) No. 51876183 and the Society of Fire Protection Engineers (SFPE) Educational & Scientific Foundation. Authors thank Dr Supan Wang (Nanjing Tech University) for helping conduct thermal analysis of the tissue paper.

References

[1] S.E. Caton, R.S.P. Hakes, D.J. Gorham, A. Zhou, M.J. Gollner, Review of Pathways for Building Fire Spread in the Wildland Urban Interface Part I : Exposure Conditions, Fire Technology. 53 (2017) 429–473. https://doi.org/10.1007/s10694-016-0589-z.

[2] A.C. Fernandez-Pello, Wildland fire spot ignition by sparks and firebrands, Fire Safety Journal. 91 (2017) 2–10. https://doi.org/10.1016/j.firesaf.2017.04.040.

[3] S.L. Manzello, S. Suzuki, M.J. Gollner, A.C. Fernandez-Pello, Role of firebrand combustion in large outdoor fire spread, Progress in Energy and Combustion Science. 76 (2020) 100801. https://doi.org/10.1016/j.pecs.2019.100801.

[4] S. Wang, X. Huang, H. Chen, N. Liu, Interaction between flaming and smouldering in hot-particle ignition of forest fuels and effects of moisture and wind, International Journal of Wildland Fire. 26 (2017)

71–81. https://doi.org/10.1071/WF16096.

[5] J.L. Urban, C.D. Zak, C. Fernandez-Pello, Cellulose spot fire ignition by hot metal particles, Proceedings of the Combustion Institute. 35 (2015) 2707–2714. https://doi.org/10.1016/j.proci.2014.05.081.

[6] P. Sun, S. Lin, X. Huang, Ignition of thin fuel by thermoplastic drips: An experimental study for the dripping ignition theory, Fire Safety Journal. 115 (2020) 103006. https://doi.org/10.1016/j.firesaf.2020.103006.

[7] T. Kashiwagi, Experimental observation of radiative ignition mechanisms, Combustion and Flame. 34 (1979) 231–244. https://doi.org/10.1016/0010-2180(79)90098-1.

[8] T. Kashiwagi, Effects of sample orientation on radiative ignition, Combustion and Flame. 44 (1982) 223–245. https://doi.org/10.1016/0010-2180(82)90075-X.

[9] D.L. Simms, Experiments on the ignition on celluslosic materials by thermal radiation, Combustion and Flame. 5 (1961) 369–375. https://doi.org/10.1016/0010-2180(61)90118-3.

[10] S. Martin, Diffusion-controlled ignition of cellulosic materials by intense radiant energy, Symposium (International) on Combustion. 10 (1965) 877–896. https://doi.org/10.1016/S0082-0784(65)80232-6.

[11] H. Zhang, Y. Qiao, H. Chen, N. Liu, L. Zhang, X. Xie, Experimental study on flaming ignition of pine needles by simulated lightning discharge, Fire Safety Journal. (2020) 103029. https://doi.org/10.1016/j.firesaf.2020.103029.

[12] A.M. Grishin, A.N. Golovanov, V. V. Medvedev, On the ignition of a layer of combustible forest materials by light radiation, Combustion, Explosion and Shock Waves. 35 (1999) 618–621. https://doi.org/10.1007/BF02674534.

[13] D.W. Warren, Optical Modeling of Fire Hazards Arising from Sunlight Focused by Water, Fire Technology. 50 (2014) 1327–1334. https://doi.org/10.1007/s10694-013-0353-6.

[14] J.D. Engerer, A.L. Brown, J.M. Christian, Ignition and damage thresholds of materials at extreme incident radiative heat flux, 2018 Joint Thermophysics and Heat Transfer Conference. (2018) 1–27. https://doi.org/10.2514/6.2018-3764.

[15] A.L. Brown, J.D. Engerer, A.J. Ricks, J. Christian, J. Yellowhair, Datasets for material ignition from high radiant flux, Fire Safety Journal. (2020) 103131. https://doi.org/10.1016/j.firesaf.2020.103131.

[16] B.M. Goldstone, Hazards from the concentration of solar radiation by textured window glass, HMSO, London, 1982.

[17] K.S. Van Dyke, THE FISH BOWL AS A FIRE HAZARD, Science. 86 (1937) 122–123. https://doi.org/10.1126/science.86.2223.122-a.

[18] Wildfire in Guilin caused by a plastic bottle, Guilinlife. (2019).

[19] Brigade step up sunlight warning after another refraction blaze, London Fire Brigade. (2015).

[20] Y. Lizhong, Z. Yupeng, W. Yafei, D. Jiakun, D. Zhihua, Z. Xiaodong, Autoignition of solid combustibles subjected to a uniform incident heat flux: The effect of distance from the radiation source, Combustion and Flame. 158 (2011) 1015–1017. https://doi.org/10.1016/j.combustflame.2011.01.008.

[21] Y. Nakamura, T. Kashiwagi, Effects of sample orientation on nonpiloted ignition of thin poly(methyl methacrylate) sheet by a laser: 1. Theoretical prediction, Combustion and Flame. 141 (2005) 149–169. https://doi.org/10.1016/j.combustflame.2004.12.014.

[22] H. Gotoda, S.L. Manzello, Y. Saso, T. Kashiwagi, Effects of sample orientation on nonpiloted ignition of thin poly(methyl methacrylate) sheets by a laser. 2. Experimental results, Combustion and Flame. 145 (2006) 820–835. https://doi.org/10.1016/j.combustflame.2006.01.008.

[23] D. Drysdale, An Introduction to Fire Dynamics, 3rd ed., John Wiley & Sons, Ltd, Chichester, UK, 2011. https://doi.org/10.1002/9781119975465.

[24] G. Rein, Smoldering Combustion, SFPE Handbook of Fire Protection Engineering. 2014 (2014) 581–603. https://doi.org/10.1007/978-1-4939-2565-0_19.

[25] J.G. Quintiere, Fundamentals of fire phenomena, John Wiley, 2006. https://doi.org/10.1002/0470091150.
[26] G. Rein, Smouldering Fires and Natural Fuels, in: Claire M. Belcher (Ed.), Fire Phenomena in the Earth System, John Wiley & Sons, Ltd., New York, 2013: pp. 15–34. https://doi.org/10.1002/9781118529539.ch2.
[27] J.L. Urban, J. Song, S. Santamaria, C. Fernandez-Pello, Ignition of a spot smolder in a moist fuel bed by a firebrand, Fire Safety Journal. 108 (2019) 102833. https://doi.org/10.1016/j.firesaf.2019.102833.
[28] S. Lin, P. Sun, X. Huang, Can peat soil support a flaming wildfire?, International Journal of Wildland Fire. 28 (2019) 601–613. https://doi.org/10.1071/WF19018.
[29] M.A. Santoso, E.G. Christensen, J. Yang, G. Rein, Review of the Transition From Smouldering to Flaming Combustion in Wildfires, Frontiers in Mechanical Engineering. 5 (2019). https://doi.org/10.3389/fmech.2019.00049.
[30] S. Lin, X. Huang, Quenching of smoldering: Effect of wall cooling on extinction, Proceedings of the Combustion Institute. 38 (2021) 5015–5022. https://doi.org/10.1016/j.proci.2020.05.017.
[31] Springer Handbook of Lasers and Optics, 2007. https://doi.org/10.1007/978-0-387-30420-5.
[32] TracePro, Software for design and analysis of illumination and optical systems., (n.d.). https://lambdares.com/tracepro/.
[33] G. Kopp, J.L. Lean, A new, lower value of total solar irradiance: Evidence and climate significance, Geophysical Research Letters. (2011). https://doi.org/10.1029/2010GL045777.
[34] M. Avendaño-Alejo, L. Castañeda, I. Moreno, Properties of caustics produced by a positive lens: meridional rays, Journal of the Optical Society of America A. (2010). https://doi.org/10.1364/josaa.27.002252.
[35] D.W. Hosmer, S. Lemeshow, R.X. Sturdivant, Applied Logistic Regression: Third Edition, 2013. https://doi.org/10.1002/9781118548387.
[36] N. Boonmee, J.G. Quintiere, Glowing ignition of wood: The onset of surface combustion, Proceedings of the Combustion Institute. 30 II (2005) 2303–2310. https://doi.org/10.1016/j.proci.2004.07.022.
[37] S. Wang, P. Ding, S. Lin, J. Gong, X. Huang, Smoldering and Flaming of Disc Wood Particles Under External Radiation: Autoignition and Size Effect, Frontiers in Mechanical Engineering. 7 (2021) 1–11. https://doi.org/10.3389/fmech.2021.686638.
[38] X. Huang, J. Gao, A review of near-limit opposed fire spread, Fire Safety Journal. 120 (2021) 103141. https://doi.org/10.1016/j.firesaf.2020.103141.
[39] F.P. Incropera, Principles of heat and mass transfer, John Wiley, 2007.
[40] Thomas James, Thermal Properties of Paper, SCIENCING. (2017).

Appendix

For the thermogravimetric analysis (TGA) test, the tissue paper was first pulverized into powders. Test was conducted with a PerkinElmer STA 6000 Simultaneous Thermal Analyzer. The initial mass was about 3 mg, and samples were heated at the constant rates of 10 K/min. Two oxygen concentrations were selected, 0% (nitrogen) and 21% (air), with a flow rate of 50 mL/min. Experiments were repeated twice for each case, and good repeatability is shown. Fig. A1 shows the (a) mass fraction and (b) normalized mass loss rate curves of this tissue paper. As indicated by the fast decrease of remaining mass fraction or the increase of mass loss rate, the thermal and oxidative decomposition of cotton starts at about 250 ℃.

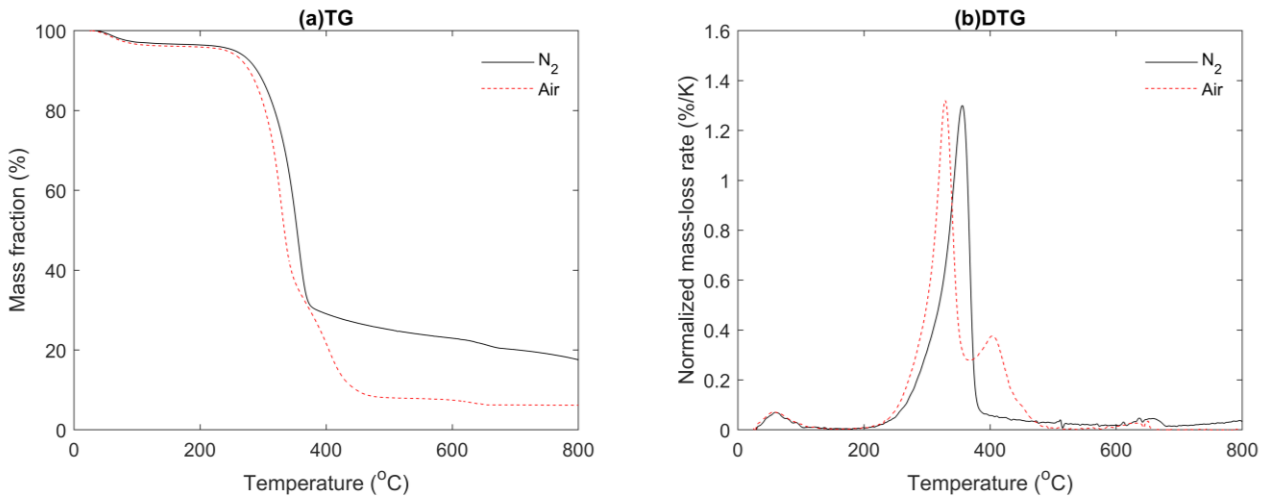

Fig. A1. TGA results of the tissue paper at a heating rate of 10 K/min.

Fig. A2 shows the simulated concentration factor (C) at different axial distances from the crown glass sphere. To verify the simulated results, the conventional radiometer was used to measure the concentrated irradiation heat fluxes of large spots up to 200 kW/m^2 and the converted concentration factors calculated by Eq. (1) are also compared in Fig. A2. Clearly, a good agreement verifies the accuracy of the irradiation heat flux from the optical simulation.

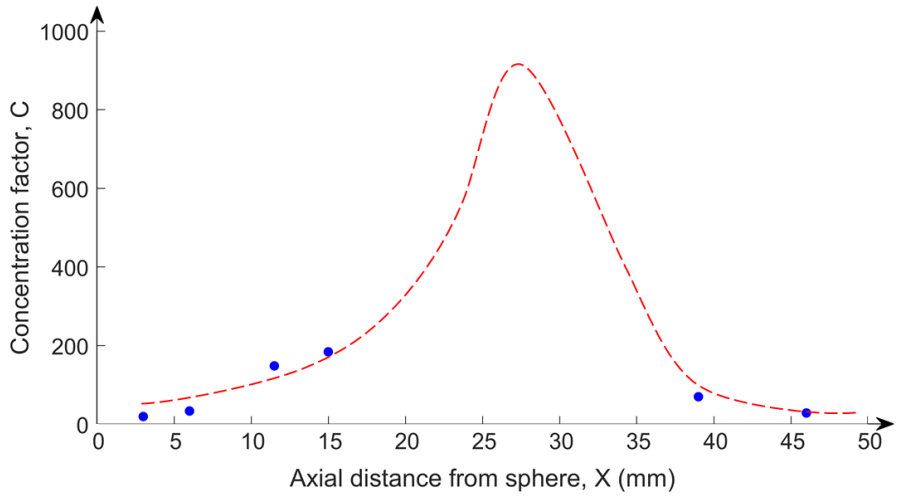

Fig. A2. Comparison of concentration factor (C) from the optical simulation and the converted values from the radiometer measurement (up to 200 kW/m^2).

The experimental data were analyzed with a machine learning method based on logistic regression and decision boundary to find the critical ignition heat flux for spotting smoldering ignition under different heating diameter. The possibility of ignition, $h_\theta(x)$, could be represented by a sigmoid function:

$$h_\theta(x) = \frac{1}{1 + e^{-\theta^T x}} \qquad (A1)$$

where θ stands for the estimated parameter vector and X is the vector of variables considered. In the case of binary classification, when $h_\theta(x) \geq 0.5$, it is considered a successful ignition and vice versa when $h_\theta(x) < 0.5$. Thus, the ideal decision boundary could be identified as $h_\theta(x) = 0.5$, and $\theta^T x = 0$.

The loss function and the sample loss sum could be written as:

$$cost(h_\theta(x), y) = -ylog\big(h_\theta(x)\big) - (1-y)\log\big(1-h_\theta(x)\big) \quad (A2)$$

$$J(\theta) = \frac{1}{m}\sum_{i=1}^{m} cost(h_\theta(x), y) \quad (A3)$$

To find the best fitting θ for the linear boundary, simple gradient descent method is applied. By adjusting the learning factor and step length in Matlab, we could generate the slope for each experiment case from 1.5 mm to 20.0 mm. To evaluate the performance of this classification model, AUC - ROC curve is further applied, which measures how much the model is capable of distinguishing between classes based on TPR (True Positive Rate) and FPR (False Positive Rate) [35]. ROC (Receiver Operating Characteristics) is a probability curve and AUC (Area Under the Curve) represents the degree or measure of separability. If a model has an AUC between 0.8 and 1, it is recognized as a high performance model with excellent or outstanding discrimination [35].

TPR and FPR could be calculated as:

$$TPR = \frac{TP}{TP+FN}, \qquad FPR = \frac{TN}{TN+FP} \quad (A4)$$

where TP, TN, FP, FN stand for True Positive, True Negative, False Positive and False Negative. As shown in Fig. A3, the simulated optimal threshold and AUC of each set is shaded with corresponding color for easier identification, with an average value of 0.86, proved to be a reliable method.

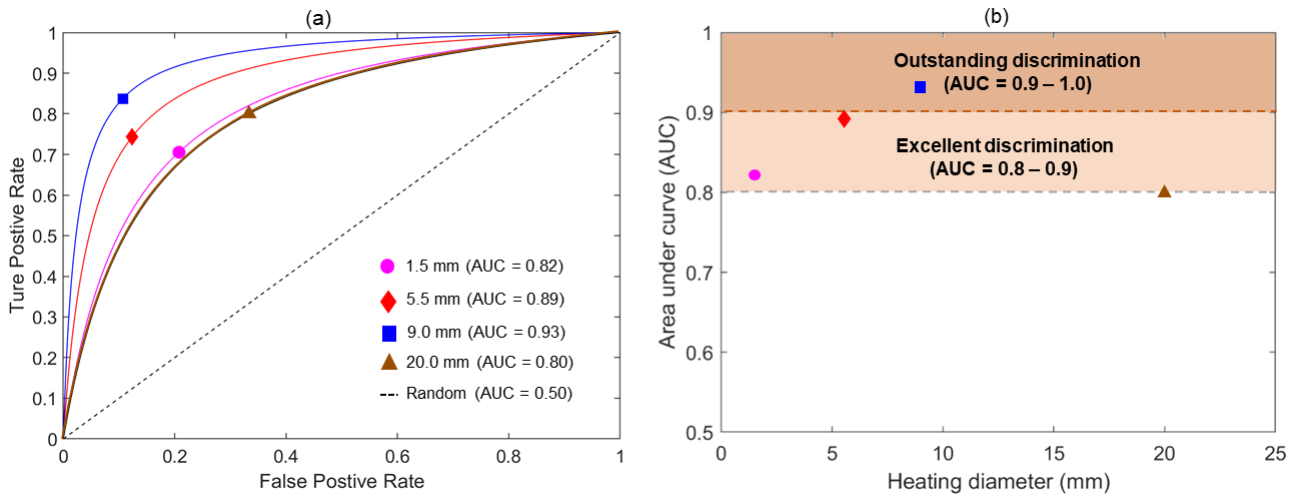

Fig. A3. (a) The simulated threshold and area under curve (AUC) for different experiment case, represented by receiver operating characteristic curves (ROC); and (b) the model performance based on AUC value comparison [33]. When AUC value is between 0.8 and 1, the model is considered to have outstanding or excellent discrimination.